View metadata, citation and similar papers at core.ac.uk

brought to you by CORE

provided by Elsevier - Publisher Connector

Available online at www.sciencedirect.com

ScienceDirect

Procedia Engineering 2 (2010) 931–940

Procedia Engineering

www.elsevier.com/locate/procedia

Fatigue 2010

Initiation and Propagation of Short Fatigue Cracks in Forged Ti6Al4V

Helge Knobbe[a,]*, Philipp Köster[b], Hans-Jürgen Christ[a], Claus-Peter Fritzen[b], Martin Riedler[c]

[a]*Institut für Werkstofftechnik, 57068 Siegen, Germany*
[b]*Institut für Mechanik und Regelungstechnik – Mechatronik, 57068 Siegen, Germany*
[c]*Böhler Schmiedetechnik GmbH & Co KG, Mariazeller Straße 25, 8605 Kapfenberg, Austria*

Received 26 February 2010; revised 11 March 2010; accepted 15 March 2010

Abstract

Forged Ti6Al4V alloy in two different microstructures was used for investigations on fatigue behaviour with special focus on crack initiation and short crack propagation characteristics. Both microstructures are in the bi-modal condition containing different amounts and sizes of primary alpha grains. Interrupted fatigue experiments were carried out using a servohydraulic test facility. Different stress levels were imposed at a constant R ratio of -1 and a frequency of 20Hz with a sinusoidal command signal. SEM together with the EBSD technique was applied for the crack observation as well as for the determination of local crystallographic orientation data with the objective of linking initiation sites and crack paths to microstructural features. It was found that most of the cracks initiate on boundaries between two lamellae in favourably oriented colonies. These cracks propagate on prismatic glide planes with high Schmid factors until they reach another boundary. In some cases crack splitting was observed leading to crack propagation in different directions on different slip planes resulting in a reduction of crack growth rate. The crack paths can be attributed either to prismatic slip planes or the basal slip plane, whereas basal slip was found inside the lamellae or in primary alpha grains. Crack deflection at boundaries is also a common feature, and is probably related to high tilt and twist angles between the grains involved.
© 2010 Published by Elsevier Ltd. Open access under CC BY-NC-ND license.

Keywords: crack initiation; crack propagation; titanium alloys; fatigue; EBSD

1. Introduction

Titanium and its alloys possess many beneficial characteristics including excellent mechanical properties, unrivalled corrosion resistance and outstanding biocompatibility [1]. This is why their usage is found in many different fields varying from industrial and automotive to medical and consumer applications. Nevertheless, the most important applications are still found within the aerospace industry, where airframes and aero engine components are made of titanium alloys [2]. These employments are mainly driven by the superior structural efficiency of these alloys caused by their high strength together with low density. The new Boeing 787 Dreamliner

* Corresponding author. Tel.: +49-271-740-3422; fax: +49-271-740-2545.
E-mail address: helge.knobbe@uni-siegen.de.

1877-7058 © 2010 Published by Elsevier Ltd. Open access under CC BY-NC-ND license.
doi:10.1016/j.proeng.2010.03.101

will contain 15% (by weight) of titanium due to the better corrosion compatibility of titanium with carbon composites (in relation to aluminum or steel), which are nowadays commonly used in modern airplane construction. But also a selection of high strength titanium forgings in the internal structure will be found in the plane [3].

A proper fatigue assessment is of course a crucial requirement for all structural components in flight service, since fatigue loading conditions always occur in these assemblies. Many approaches only consider the propagation of long cracks (damage tolerant approach) and thus make use of phenomenological equations such as Paris Law in classical linear elastic fracture mechanics [4]. As an alternative, total life approaches are used with S-N curves as basis for a fatigue life prediction according to Basquin/Coffin/Manson [5–7]. These methods do generally not distinguish between crack initiation, short crack propagation and long crack propagation, which might be important in some cases. Another option, which is linked to physical properties of the material, is a microstructural-based short fatigue crack propagation model for lifetime prediction [8]. Since the loads arising in components associated with the internal structure are usually in the area of high cycle fatigue, up to 99% of the total lifetime can be spent with crack initiation and the propagation of short fatigue cracks [9]. Thus, modeling short crack propagation in virtual microstructures promises a flexible and reliable approach for lifetime calculations. This paper concentrates on the experimental investigations which are necessary in order to establish and verify the model described in [10]. Mainly two kinds of experiments were conducted; (i) constant load fatigue experiments for collecting SN-data and (ii) interrupted constant load fatigue experiments in order to gain knowledge on crack initiation and short crack propagation linked with local microstructural features.

2. Material and Experimental

2.1. Material

The Ti6Al4V alloy under investigation was delivered by Böhler Schmiedetechnik, where round bar stocks were forged into "v-shaped" pieces from which all specimens were machined. Two different heat treatments were applied after the forging process, (i) mill-annealing (MA) and (ii) solution heat treatment (SHT).

The most important chemical elements of the composition are given in Tab. 1. The analysis was done using spark emission spectroscopy. The figures represent mean values from three measurements and are within normal scatter. Some Fe content was found probably resulting from impurities of the alloying elements or from the process routine.

Table 1. Chemical composition in wt.%

Element	Al	V	Fe	Ti
wt. %	6.5	3.52	0.133	bal.

Micrographs using a scanning electron microscope with backscattered electron detector giving a channeling grain contrast of the resulting microstructures are shown in Fig. 1. A typical bi-modal microstructure was obtained in both conditions, thus no distinctive differences are present. The microstructures consist of primary alpha grains (α_p-grains) and colonies of secondary alpha lamellae (α_s-lamellae). A little content of remaining β-phase (app. 5–8%) can be found between the lamellae or at triple points.

The primary alpha grains of the SHT microstructure are fully recrystallized due to the applied dwell time at a high temperature near the forging temperature, while the MA condition was cooled directly after forging, so some grains are only partially recrystallized. This can be deduced from orientation measurement data exhibiting large misorientation variations in single primary alpha grains along with sub grain boundaries (see section 3 for a detailed description).

The final heat treatment step was the same for both microstructures consisting of a plain stress relieving annealing above the Ti_3Al solvus temperature. The phase fractions are slightly different (α_p: 71% MA, 61% SHT), and the mean grain sizes are in the same magnitude (α_p: 10µm MA, 9µm SHT; α_s: 7µm MA, 9µm SHT). It should be mentioned that no subgrains were accounted for in the MA condition and that the α_s size refers to the colonies,

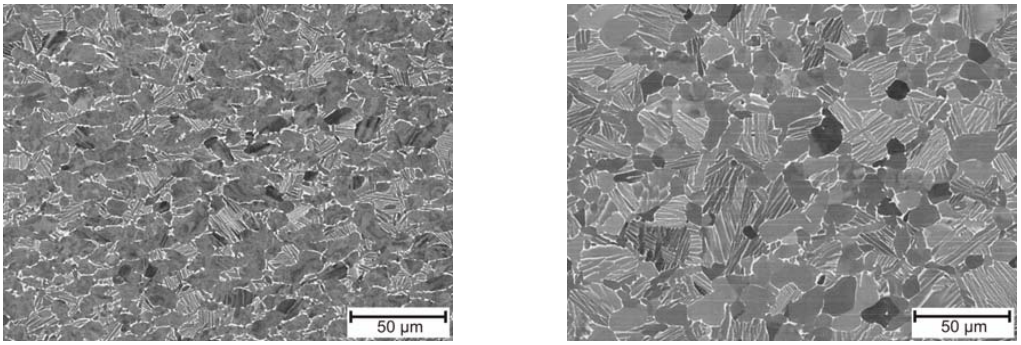

(a) (b)

Fig. 1. Microstructure of (a) MA condition and (b) SHT condition.

meaning lamellae of the same orientation. Of course the mean lamella thickness is much smaller in case of the MA condition.

2.2. Experimental

All specimens except of the micro-sections were electro-chemically polished in a solution of perchloric acid and methanol prior to testing to meet the requirements for electron backscattered diffraction (EBSD) experiments. The surface should be as smooth as possible without any residual stresses from machining. This requirement can be perfectly met by grinding and vibration polishing (which was done in case of flat specimens for micro-sections), but is impossible for cylindrical specimens, where electrolytic polishing is the only possibility available. It should be pointed out that a slight surface roughness results from different metal removal rates of the different phases. The topography, measured by atomic force microscopy (AFM), was about 400nm from peak to valley.

Fatigue experiments were carried out in symmetrical push-pull with a servohydraulic MTS 810 test system under load control at a frequency of 20 Hz. All experiments were stopped by specimen failure or at 6×10^6 cycles. The samples which survived this number of cycles are referred to as run-out specimens. Cylindrical specimens with a milled shallow notch in the gauge length were used for the crack initiation and short crack growth investigations in order to limit the area to be observed. Some tests were interrupted after certain numbers of cycles to enable studying several cracks in the scanning electron microscope (SEM) together with EBSD. A Philips XL30 microscope equipped with automated orientation imaging microscopy (OIM^{TM}) was employed for all analytical research work.

3. Results and Discussion

3.1. EBSD measurements

Prior to the description of the results, it seems adequate to compare both microstructures by EBSD measurements to illustrate the differences and peculiarities. Fig. 2 shows EBSD data from MA condition (Fig. 2a) and SHT condition (Fig. 2b) in terms of inverse pole figures overlaid with pattern quality. Every color represents an orientation according to the legend in Fig. 2c, whereas the overlaid grayscale is a measure for the quality of each diffraction pattern; the darker the grayscale the poorer the quality. The pattern quality depends on specimen preparation and condition as well as on microstructural features such as phase and grain boundaries. It usually gets worse near boundaries because patterns begin to overlap and this reduces the quality. An advantage of this fact is that this quantity can be used to distinguish between single lamellae in one colony, where the orientation is the same. A comparison of Fig. 2a with Fig. 2b demonstrates the difference in lamella size.

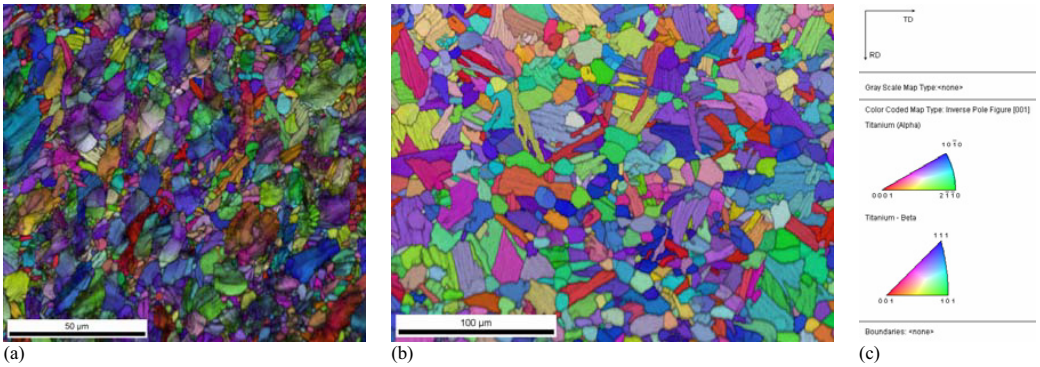

(a) (b) (c)

Fig. 2. Inverse pole figure with pattern quality overlay of (a) MA condition; (b) SHT condition; (c) legend of color code.

Furthermore, the presence of elastic and plastic strains (or in other words high dislocation densities) also has a great influence on the pattern quality leading to ambiguous and blurred patterns [11]. This can be seen in some α_p grains of the MA condition, where the color is overlaid with a shady grayscale. This feature is not observed in the SHT condition. Another difference showing the same phenomenon can be observed when considering the color gradients in some α_p grains. These variations in orientation represent the residual strains and crystal rotations; again this is not present in the SHT condition.

A deeper analysis of the misorientation variation is given by Fig. 3 where an evaluation was done for a single grain. Fig. 3a shows the pattern quality clearly revealing some areas with very poor quality presumably linked with sub-grain boundaries and high dislocation densities.

This conclusion is confirmed by Fig. 3b where the inverse pole figure of the grain is plotted showing a color gradient over a broad range of orientations. Very recently these lattice curvatures have been used to determine the geometrically necessary dislocations (GND) and even distinguish between different types of GND, see [11].

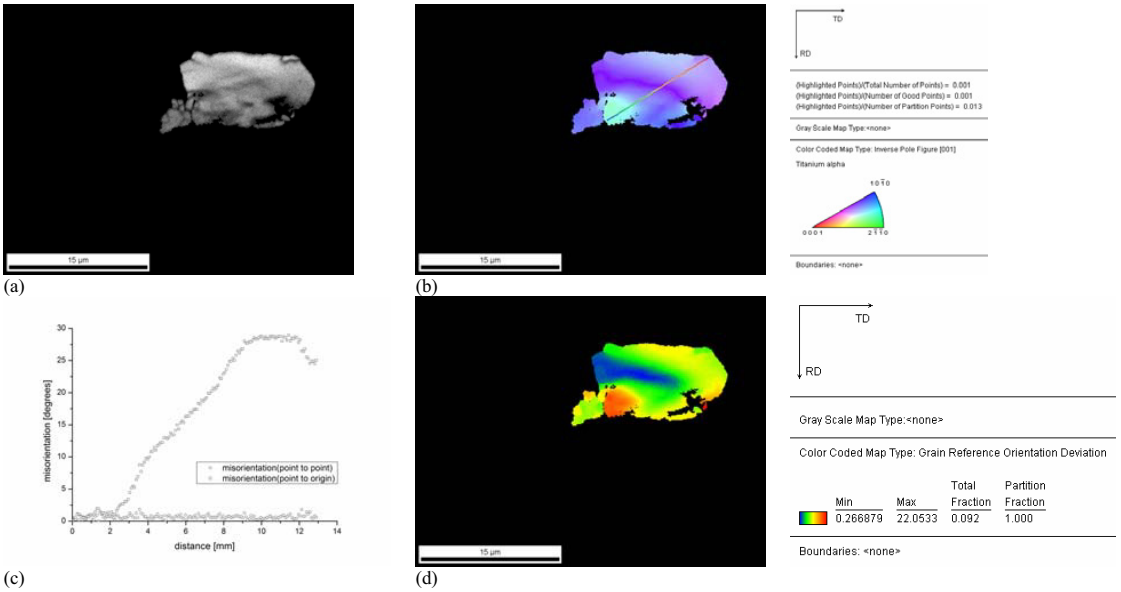

(a) (b) (c) (d)

Fig. 3. Detailed EBSD measurements on one grain: (a) pattern quality and (b) inverse pole figure showing sub-grain boundaries; (c) local misorientation plot along the colored line in (b); (d) local misorientation.

Table 2. Tensile behavior of the two heat treatment conditions

Condition	Young's Modulus [GPa]	Yield Strength (0.01%) [MPa]	Yield Strength (0.2%) [MPa]	UTS [MPa]	Elongation [%]
MA	116	790	948	987	12
SHT	117	781	878	942	11

The linear misorientation along the colored line shown in Fig. 3b is presented in Fig. 3c. Two different charts are shown. The more or less horizontal line (open circles) is the point to point misorientation, whereas the open quads represent the point to origin misorientation. It is obvious that a continuous change in orientation is present, no peaks are observed in both plots. The point to origin chart indicates a misorientation as high as 30° in maximum. Fig. 3d shows the orientation deviation with respect to a reference orientation, which is the calculated mean orientation of the grain, giving maximum deviations of 22°. This maximum is found in the turquoise region; see Fig. 3b. Obviously, this is an example of a heavily deformed α_p grain. It even might contain a rather large sub grain, marked by the red/orange area in Fig 3d, together with some smaller sub grains in the lower left area of the grain.

3.2. Tensile Test

In order to compare the two microstructures, uniaxial tensile tests were conducted. The mean values of three different tests are summarized in Tab. 2. It is obvious that the differences are not very pronounced since the microstructural morphology (primary globular and secondary lamellar alpha grains) was not changed. Young's modulus and elongation at fracture are the same, but the elastic limit (at least for 0.2% plastic strain) together with the ultimate tensile strength (UTS) is perceptibly increased in case of the MA microstructure (+7% Yield Strength; +5% UTS). This increase can be attributed to the smaller lamella size resulting in a higher grain/phase boundary density. According to Hall [12] and Petch [13] grain or phase boundaries cause dislocation pile-ups during plastic deformation. A higher strength can thus be the result of a finer microstructure according to the Hall-Petch relation. Another aspect is probably the remaining elastic and plastic strain from the forging process. A high dislocation density as it is apparent in unrecrystallized α_p-grains is supposed to strengthen the material.

3.3. Fatigue Behavior

The fatigue behavior was characterized by constant-stress amplitude experiments in order to obtain SN-curves. The corresponding data for both microstructures is plotted in Fig. 4 in which the open quads and the open circles represent the MA condition and the SHT condition, respectively. The arrows indicate run-out specimens which survived 6×10^6 cycles without failure.

Two regions can be distinguished. In the stress amplitude region between 700 and 600 MPa almost no difference is evident for the two microstructures because the circles and the quads lie in the same scatter band. As the classical fatigue limit is approached some differences appear: (i) the fatigue limit of the MA condition is higher than the one of the SHT condition (the increase is about 50 MPa (500 MPa for MA; 450 MPa for SHT)) and (ii) the scatter of the cycles to failure for the MA condition is much more pronounced, reaching almost over two decades in terms of load cycles (5×10^4 – 5×10^6 cycles), whereas for the SHT condition a precise distinction can be observed. Either the specimens fail in the range of 10^5 cycles or survive 6×10^6 cycles. Two important conclusions can be drawn from the observed behavior. Apparently, both microstructures behave very similar at higher stress levels, where the resistance against crack propagation is the determining factor for fatigue life. Once a crack has overcome the critical length for further growth the propagation rates are more or less equal for both microstructures. However, if the resistance against crack initiation or short crack propagation is the determining factor for fatigue life, which is typically the case for high cycle fatigue loading conditions, the MA microstructure yields higher values.

Similar results are summarized in [14]. As long as a crack is microstructurally short its behavior is highly influenced by local microstructural features such as grain, sub grain or phase boundaries, grain orientation, residual stresses and dislocation structures [15,16]. The SHT microstructure has no residual stresses or high dislocation densities, also no sub-grain boundaries can be found. But in addition the lamellar grains are relatively coarse raising

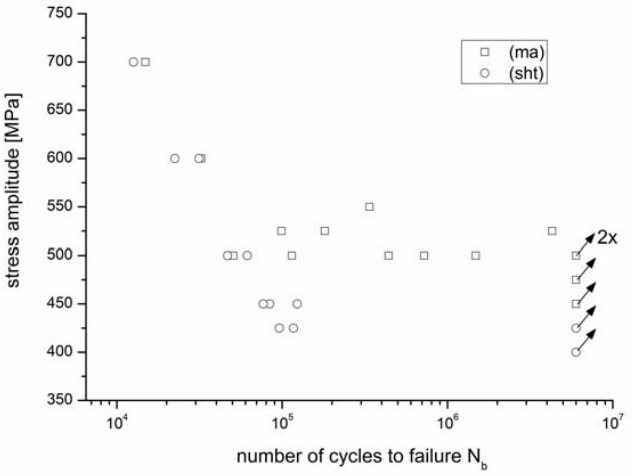

Fig. 4. SN-data for the two different microstructures.

the mean slip length. These factors reduce the crack initiation resistance. The MA condition contains finer lamellae and high dislocation densities in some primary alpha grains together with sub-grain boundaries impeding the capability of dislocations to move and thus crack initiation or short crack propagation are retarded. The gain in fatigue limit can be explained in terms of the Hall-Petch equation which also holds true in case of fatigue strength and is in good agreement with the tensile behavior. The remarkable scatter regarding the fatigue limit may be explained by the heterogeneity of the MA microstructure. It is obvious that residual stresses can impede or enhance crack initiation or short crack propagation, depending on grain orientation and internal stress distribution.

3.4. Crack Initiation / Short Crack Propagation

In order to characterize the initiation and the propagation of short fatigue cracks, the experiments were interrupted after defined numbers of load cycles for investigations in the SEM before the fatigue experiment was continued. This procedure was followed for both microstructures. Mainly two initiation mechanisms were found: (i) crack initiation in α_p grains or (ii) crack initiation in between two lamellae in α_s colonies. The latter one can be observed more often in both cases.

Fig. 5 shows an example of a crack initiated in a primary alpha grain after 5×10^3 cycles (Fig. 5a) and 10^4 cycles (Fig. 5b) in the MA microstructure. Fig. 6c contains the inverse pole figure of the area overlaid with the pattern

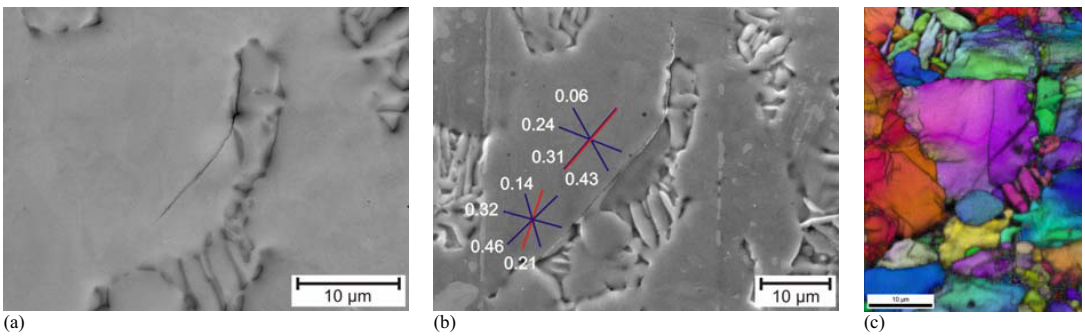

(a) (b) (c)

Fig. 5. Fatigue crack in an α_p grain in the MA microstructure after (a) 5×10^3 cycles and (b) 1×10^4 cycles; (c) shows the inverse pole figure of the area.

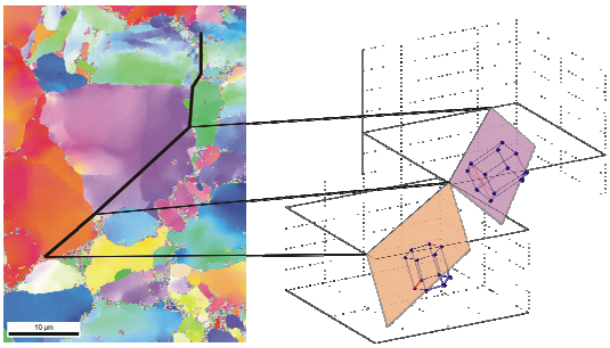

Fig. 6. 3D analysis of the slip planes activated in the primary alpha grains.

quality, again showing the internal structure together with some very small sub-grains especially in the upper part. The load axis is horizontal. In the upper part the crack follows the grain boundary (a) and propagates later on with a zigzag-like behavior (b) through the small sub-grains. In this segment it is difficult to assign single activated slip systems to the crack path. Since the propagation direction is almost rectangular to the load axis it is supposed that normal stresses are mainly responsible for the crack propagation characteristics. Nevertheless, the main part of the crack path in the middle of the micrographs is oriented approximately at an angle of 45° to the load axis. This leads to the assumption that the maximum shear stress is the crack driving force. An analysis of the EBSD data reveals that the crack path is almost parallel either to the basal plane (red lines in Fig. 6b, or one of the possible prismatic planes (blue lines in Fig. 5b. The lines represent the calculated slip traces at the surface. Both slip planes exhibit relatively high Schmid factors of 0.43 and 0.46, respectively.

Obviously, the grain boundary between the purple and the orange grain (see Fig. 5c) has easily been crossed. More detailed information provides a 3-dimensional analysis of the slip planes presented in Fig. 6. The simplified crack path is marked by the black line in the inverse pole figure. For the two grains where it was possible to assign slip systems the 3D orientation of the slip planes is given in the left part of the figure. The tilt angle and in particular the twist angle, which is the governing factor for the effectiveness of a grain boundary as obstacle against dislocation movement or crack propagation [17] are quite small. It follows from the above that cracks can easily change from one slip system to another if necessary when crossing a grain boundary, depending on the respective orientation of the grains.

Several other authors also reported crack initiation in primary alpha grains [18–21]. Usually, flat facets on the fracture surface in the vicinity of the supposed crack origin can be seen and serve as evidence for cracked α_p-grains [18,19].

The other initiation site found is between the α_s lamellae. This is also confirmed in [20]. An example of a crack found in the MA condition is presented in Fig. 7. This crack has grown along the boundary between two lamellae;

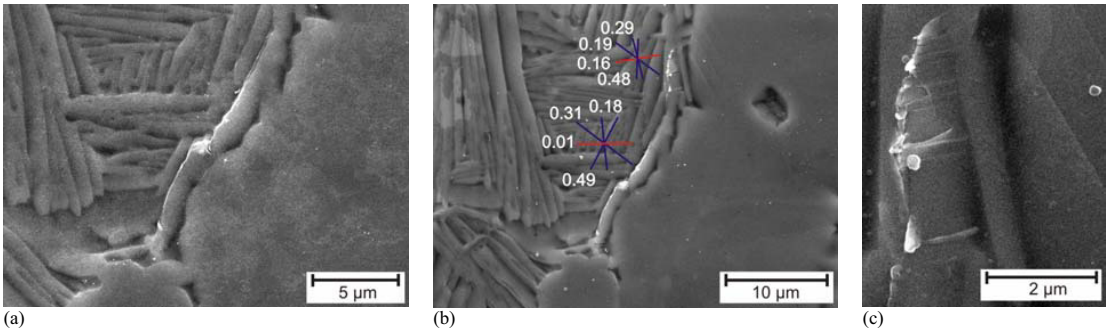

(a) (b) (c)

Fig. 7. Fatigue crack in an α_s grain in the MA microstructure after (a) 5×10^3 cycles and (b) 1×10^4 cycles; (c) shows the detail of the upper crack after 1×10^4 cycles.

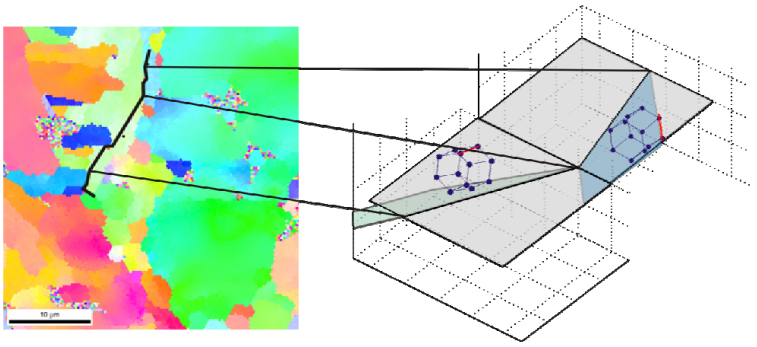

Fig. 8. 3D analysis of the slip planes activated in the lamella grains.

see part (a), which displays the crack after 5×10^3 cycles. A description of the slip systems analogous to the above is integrated in Fig. 7b showing the crack after 10^4 cycles. A detailed micrograph of the upper crack tip after 10^4 load cycles is given in Fig. 7c. Apparently, the crack initiated and grew on a prismatic slip system with a very high Schmid factor of 0.49. While crossing the boundary in the upper part, the crack begins to grow into the lamellae and several branches almost rectangular to the primary crack path have developed. A comparison with the calculated slip markings reveals that directly after growing into the lamellae a prismatic slip plane with a relatively low Schmid factor was used (0.29). Even more surprising is the development of some branches on the basal plane (red line in Fig. 7b). This plane exhibits a very low Schmid factor of 0.16. But as the crack further proceeds, it is more and more deflected in a direction of a prismatic plane with a much higher Schmid factor (0.48). The crack path shown in Fig. 7c suggests that probably more than just one slip system is activated. The rather small crack growth rate which can be derived when comparing the total crack length of part (a) with part (b) leads to the assumption that the crack consumes a lot of energy in this stage of growth, as it would be needed for the activation of multiple slip.

Another explanation why the crack propagates rather slowly can be derived from the 3D analysis of the slip planes as it is shown in Fig. 8. The twist angle is substantially large and also the slip directions are quite different from each other. This boundary seems to be fairly effective as a barrier to the fatigue damage. This is in good agreement with the slow propagation rate observed.

The crack initiation and propagation mechanisms are in principle the same in case of the SHT condition. Cracks initiate either in primary alpha grains on basal planes or in secondary alpha lamellae colonies, preferably between two lamellae on mostly prismatic slip planes. Two typical examples of cracks initiated according to these mechanisms shows Fig. 9. As can be seen in Fig. 9a a crack has formed in α_p grain under a 45° angle to the horizontal load axis on the basal planes. But cracks also grow into the lamellae as Fig. 9b shows in the upper part.

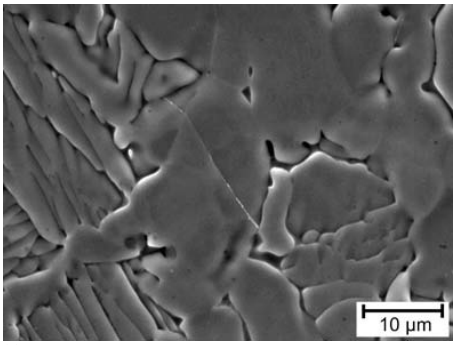

(a)

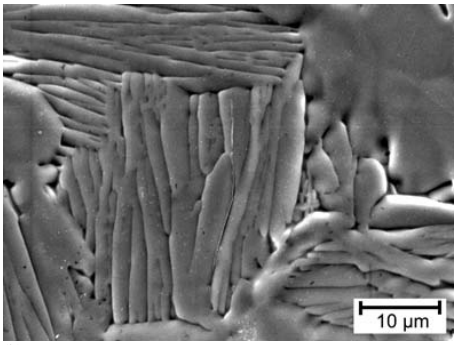

(b)

Fig. 9. Crack initiation sites in the SHT condition.

As the critical shear stresses for basal and prismatic slip do not differ too much [19], an activation of both systems is very likely to happen. Moreover, the addition of alloying elements like aluminum or interstitial oxygen leads to a reduction of the stacking fault energy on the basal planes [21]. Thus, dislocations can dissociate and their movement is increasingly restricted to these planes. This may explain the crack deflection in Fig. 7c to basal planes although the Schmid factor is low.

4. Conclusions

Some important conclusions can be drawn from the results presented in this paper. Two microstructural conditions of Ti6Al4V alloy were investigated, mill annealed and solution heat treated. Both are of bi-modal nature, but having different lamella sizes. Moreover, the mill annealed condition is only partially recrystallized, thus containing a high dislocation density. The mechanical tests and a detailed analysis of fatigue crack initiation and microstructural short crack propagation revealed the following main results:

- The MA condition has a superior mechanical behavior regarding ultimate tensile strength and fatigue limit. This is because of the finer microstructure according to the Hall-Petch relationship.
- The scatter in the region of the fatigue limit is increased for the MA condition probably due to the inhomogeneity of the microstructure resulting from elastic and plastic strains or residual stresses.
- The dominating crack initiation mechanisms are the same for both microstructures. Cracks grow on pyramidal and on basal planes either between two lamellae in a colony or in primary alpha grains.
- Cracks in lamellar regions are more likely to appear than those initiated in primary alpha grains.
- In many cases it is possible to correlate the crack path with slip systems exhibiting high Schmid factors.

Acknowledgements

The authors would like to express their gratitude to Böhler Schmiedetechnik GmbH & Co KG for financial supporting the project and supplying the material.

References

[1] Jackson M, Dring K. A review of advances in processing and metallurgy of titanium alloys. *Mat Sci Tech* 2006;**7**:881–7.

[2] Boyer RR. An overview on the use of titanium in aerospace industry. *Mat Sci Eng A* 1996;**213**:103–14.

[3] Boyer RR, Briggs RD. Presentation - The Boeing 7E7: an update. *Proc 16th Conf on advanced aerospace materials and processes* 2005.

[4] Paris PC, Gomez MP, Anderson WE. A rational analytic theory of fatigue. *Trend Eng* 1961;**13**:9–14.

[5] Basquin OH. The exponential law of endurance tests. *Proc Annual Meeting ASTM* 1919;**10**:625–34.

[6] Coffin LF. Fatigue at high temperatures. *ASTM STP520* 1973;744-782.

[7] Manson SS. Fatigue: A complex subject-some simple approximations. *J Exp Mech* 1965;**5**:193–226.

[8] Künkler B, Düber O, Köster P, Krupp U, Fritzen CP, Christ HJ. Modelling of short crack propagation – transition from stage I to stage II. *Eng Frac Mech* 2008;**75**:715–25.

[9] Tokaji K, Takafiji S, Ohya K, Kato Y, Mori K. Fatigue behavior of beta Ti-22V-4Al alloy subjected to surface-microstructural modification. *J Mat Sci* 2003;**38**:1153–59.

[10] Köster P, Knobbe H, Fritzen CP, Christ HJ, Riedler M. Simulation of Stage I-Short Crack Propagation in Forged Ti6Al4V. *Proc Eng* 2010; this issue.

[11] Britton TB, Birosca S, Preuss M, Wilkinson AJ. Electron backscatter diffraction study of dislocation content of a macrozone in hot-rolled Ti–6Al–4V alloy. *Scripta Mater* 2010;**62**:639–42.

[12] Hall EO. The deformation and aging of mild steel: II. characteristica of the Lüders deformation. *Proc Phys Soc Lond B* 1951;**64**:747–53.

[13] Petch NJ. The cleavage strength of polycrystals. *Iron Steel Inst B* 1953;**174**:25–32.

[14] Chan KS. Changes in fatigue life mechanism due to soft grains and hard particles. *Int J Fat* 2010;**32**:526–34.

[15] Zhang YH, Edwards L. On the blocking effect of grain boundaries on small crystallographic fatigue crack growth. *Mater Sci Eng A* 1994;**188**:121–31.

[16] Zhai T, Wilkinson AJ, Martin JW. A crystallographic mechanism for fatigue crack propagation through grain boundaries. *Acta Mater* 2000;**48**:4917–25.

[17] Zhang ZF, Wang ZG. Fatigue-cracking characteristics of a copper bicrystal when slip bands transfer through the grain boundary. *Mater Sci Eng A* 2003;**343**:308–17.

[18] Golden PJ, John R, Porter III WJ. Variability in room temperature fatigue life of alpha + beta processed Ti-6Al-4V. *Int J Fatigue* 2009;**31**:1764–70.

[19] Bridier F, Villechaise P, Mendez J. Slip and fatigue crack formation processes in an α/β titanium alloy in relation to crystallographic texture on different scales. *Acta Mater* 2008;**56**:3951–62.

[20] Oberwinkler B, Riedler M, Eichlseder, W. Importance of local microstructure for damage tolerant light weight design of Ti-6Al-4V forgings. *Int J Fatigue* 2010;**32**:808–14.

[21] Zaefferer S. A study of active deformation systems in titanium alloys: dependence on alloy composition and correlation with deformation texture. *Mat Sci Eng A* 2003;**344**:20–30.